Hindawi Publishing Corporation
ISRN Ceramics
Volume 2013, Article ID 369670, 12 pages
http://dx.doi.org/10.1155/2013/369670

Research Article

Electrical Conduction in $(Na_{0.5}Bi_{0.5})_{1-x}Ba_xTiO_3$ $(0 \le x \le 1)$ Ceramic by Complex Impedance/Modulus Spectroscopy

Ansu Kumar Roy, Kamal Prasad, and Ashutosh Prasad

University Department of Physics, T.M. Bhagalpur University, Bhagalpur 812007, India

Correspondence should be addressed to Ashutosh Prasad; apd.phy@gmail.com

Received 30 December 2012; Accepted 18 February 2013

Academic Editors: S.-Y. Chu, O. Dymshits, and S. Marinel

The present work describes the piezoelectric, impedance, and conductivity studies of $(Na_{0.5}Bi_{0.5})_{1-x}Ba_xTiO_3$; $(1-x)$BNT-xBT $(0 \le x \le 1)$ ceramics. The ceramics were prepared by conventional ceramic fabrication technique. X-ray diffraction data confirmed the formation of a pure compound in all the compositions. Williamson-Hall plot yielded the apparent crystallite sizes ~26–52 nm, and SEM micrograph showed grain sizes ranging between 1.8–3.5 μm for the material samples. Values of longitudinal piezoelectric charge coefficients of the samples poled under a dc electric field of about 2.5 kV/mm at 80°C/15 min indicated that their piezoelectric properties near the MPB are rather sensitive to the phase composition and reach preferred values at $x = 0.08$, where the relative content of the tetragonal phase is significantly higher than that of the monoclinic phase. Complex impedance/modulus spectroscopic analyses indicated the presence of grain-boundary effect along with the bulk contribution and also confirmed the presence of non-Debye type of multiple relaxations in the materials. The temperature dependent electrical conductivity data suggest the negative temperature coefficient of resistance behaviour. The activation energy studies allow insight into the nature of the conduction mechanisms occurring in the materials system which are explained on the basis of hopping model of charge carriers.

1. Introduction

Till date the most widely used piezoelectric materials are $PbTiO_3$-$PbZrO_3$- (PZT)based ceramics because of their excellent piezoelectric properties. In view of harmful effects for the mankind as well as for the other living creatures on the earth due to possible lead toxicity spreading during processing, the use, recycling, and disposal of devices containing PZT, a global interest has arisen in developing piezoelectric materials that are biocompatible and environment-friendly. Therefore, it is necessary to investigate and develop environment-friendly materials to replace PZT-based ceramics with comparable properties. Recently, lead-free piezoelectric ceramic materials with perovskite structure and Bi-layered structure oxides as viable alternatives to PZT have been reported. Among these materials, bismuth sodium titanate $Bi_{0.5}Na_{0.5}TiO_3$ (BNT), first reported by Smolenskii et al. [1], is considered to be a viable candidate to replace the widely used lead-based perovskite materials due to its high remnant polarization ($P_r = 38\,\mu C/cm^2$). Nevertheless, the applications of BNT are limited by its high coercive field ($E_c = 7.3$ kV/mm) and high conductivity. It is an A-site substituted distorted perovskite compound (ABO_3). Its dielectric properties reveal two anomalies. The well-known first one corresponds to the antiferroelectric-paraelectric transition at about 320°C [2]. The other one at ~150°C–200°C is frequency-dependent (called the depolarization temperature, T_d) and is not yet well understood, since no structural transition is observed at that temperature. In order to improve the poling process and enhance the piezoelectric properties of the BNT ceramics, a number of BNT-based solid solutions, such as BNT-$BaTiO_3$(BT) [3, 4], BNT-$Bi_{0.5}K_{0.5}TiO_3$ [5], BNT-(Ba, Sr)TiO_3 [6], BNT-$SrTiO_3$-$Bi_{0.5}Li_{0.5}TiO_3$ [7], BNT-$Bi_{0.5}K_{0.5}TiO_3$-$Bi_{0.5}Li_{0.5}TiO_3$ [8], BNT-$Bi_{0.5}K_{0.5}TiO_3$-$BiFeO_3$ [9], BNT-BT-$Bi_{0.5}K_{0.5}TiO_3$ [10], BNT-BT-$KNbO_3$ [11], Bi_2O_3 doped BNT-BT [12], BNT-$NaNbO_3$ [13], BNT-$BiFeO_3$[14], BNT-Bi_2O_3-Sc_2O_3 [15], BNT-La_2O_3 [16], and BNT-$Ba(W_{1/2}Cu_{1/2})O_3$ [17], and so forth have been developed and studied in recent years. It is found that the dielectric and piezoelectric properties of these "modified" BNT-based materials were effectively enhanced when the morphotropic phase boundary (MPB) composition (in which coexistence of

(rhombohedral/monoclinic) tetragonal phases was assumed) was attained. Many of the researchers from all over the world have reported the MPB composition to lie within $x = 0.05$–0.08 for $(1 - x)$BNT-xBT. A recent literature has reported an exhaustive study on $(1 - x)$BNT-xBT [18]. However, in view of some of the important and yet untouched aspects and properties of the $(1 - x)$BNT-xBT ceramic system, the present work is aimed at studying the piezoelectric properties, impedance/modulus spectroscopy and conductivity of the $(1 - x)$BNT-xBT($x = 0$, 0.02, 0.04, 0.05, 0.06, 0.08, 0.10, and 1.0) ceramic system. By knowing the conduction mechanism within a material system, we can tune their properties and can use them for particular applications. In this context, the present study of $(Na_{0.5}Bi_{0.5})_{1-x}Ba_xTiO_3(1 - x)$BNT-$x$BT ($0 \leq x \leq 1$) ceramics is assumed worthwhile in probing the conduction mechanism in detail which may be helpful in tailoring the electrical characteristics for desired applications.

2. Experimental

Polycrystalline samples having the nominal formula $(Bi_{0.5}Na_{0.5})_{1-x}Ba_xTiO_3$; $(1 - x)$BNT-xBT were prepared by a high temperature solid-state reaction technique using oxides Bi_2O_3, Na_2CO_3, $BaCO_3$ and TiO_2 (HiMedia) (having a purity of more than 99.5% for each of them) in a suitable stoichiometry. The above ingredients were mixed thoroughly, first in air and then in methanol medium using agate mortar and pestle. The oxide mixtures were calcined at an optimized temperature of 1170°C for about 3 h in an alumina crucible. Then, by adding a small amount of polyvinyl alcohol (PVA) as a binder to the calcined powder, circular and rectangular disk-shaped pellets were fabricated for different compositions by applying uniaxial pressure of 4–6 tons per square inch. The pellets were subsequently sintered at an optimized temperature of 1180°C for about 2 h. The XRD spectra were taken on calcined powders of $(1 - x)$BNT-xBT with an X-ray diffractometer (X'PERT-PRO, Pan Analytical, USA) at room temperature, using CuK_α radiation ($\lambda = 1.5405$ Å) over a wide range of the Bragg angles ($20^\circ \leq 2\theta \leq 80^\circ$). The microstructure of the sintered pellets was observed at room temperature from the micrographs obtained by using a scanning electron microscope (JEOL-JSM840A). The temperature-dependent dielectric constant (ε'), loss tangent ($\tan\delta$), impedance, and phase values at various frequencies like 100 Hz, 1 kHz, 10 kHz, 100 kHz, and 1 MHz were evaluated using the capacitance, impedance, and phase data obtained from a computer-controlled LCR Hi-Tester (HIOKI 3532-50, Japan) on a symmetrical cell of type AgceramicAg, where Ag is a conductive paint coated on either side of the pellet. Longitudinal piezoelectric charge coefficients (d_{33}) of the poled $(1 - x)$BNT-xBT ceramic samples were measured under an electric field of about 2.5 kV/mm at 80°C/15 min in a silicone oil bath using a PM3500 d_{33}/d_{31} meter (KCF Technologies, USA).

3. Results and Discussion

3.1. Structural Study. Figure 1 shows the XRD patterns of calcined $(1 - x)$BNT-xBT powder. A standard computer program (POWD) was utilized for the XRD-profile analysis. Good agreement between the observed and calculated interplanar spacing without any trace of extra peaks due to the constituent oxides was found, thereby suggesting the formation of a biphasic pure compound. All the reflection peaks of the XRD pattern of the samples were indexed, and the lattice parameters were determined in the monoclinic as well as in tetragonal system of crystals. The presence of monoclinic and tetragonal phases in the compositions having $x \leq 0.06$ and $x \geq 0.06$, possibly due to its constituents BNT and BT, respectively, is endorsed by the splitting of peaks 44.5°–47.5° into two peaks (200) and (002) in the XRD patterns, as shown in Figures 1(a) and 1(b). This splitting becomes increasingly prominent with the further addition of BT for 0.92 BNT-0.08 BT, 0.90 BNT-0.10 BT as well as for pure barium titanate (BT). The apparent particle size and lattice strain of $(1 - x)$BNT-xBT were estimated by analyzing the X-ray diffraction peak broadening, using the Williamson-Hall approach [19]:

$$\beta \operatorname{Cos}\theta = 2\left(\frac{\Delta\xi}{\xi}\right)\sin\theta + \frac{K\lambda}{D}, \tag{1}$$

where D is the crystallite size, β is the diffraction peak width at half intensity (FWHM), $\Delta\xi/\xi$ is the lattice strain, and K the Scherrer constant (~0.89). However, these results have not been shown in the paper for brevity sake.

3.2. Tolerance Factor. In general, the perovskite structure is stable in the region $0.880 < t < 1.090$ [18], and the stability is higher as the t-value is closer to 1. For example, the t-value of a cubic $SrTiO_3$ (= 1.001) is closer to 1 than that for the orthorhombic $CaTiO_3$ (= 0.966). The t-value also provides an indication about how far the atoms can deviate from the ideal packing positions and be still "tolerated" in the perovskite structure. Calculated values of tolerance factors for different $(1 - x)$BNT-xBT compositions ($x = 0$, 0 02, 0. 04, 0.05, 0.06, 0.08 and 1) using the Goldschmidt formula [20] are very close to 1, (lying between minimum = 0.985 for BNT and maximum = 1.058 for 0.90 BNT-0.10 BT), thus indicating a good stability for all the test samples of the present work.

3.3. Microstructural Study. Figure 2 shows the SEM micrograph of $(1 - x)$BNT-xBT ($x = 0$, 0. 02, 0.04, 0.05, 0.06, 0.08, and 1) compositions. Grain shapes are clearly visible, thereby indicating the existence of polycrystalline microstructure. Grains of unequal sizes with less porosity appear to be distributed throughout the samples. The average grain size was found with the help of linear intercept method. Grain sizes for the chosen compositions were found to range 1.8–3.5 μm, generally decreasing with increasing barium titanate content, as detailed in Table 1. Of these, the 0.96 BNT-0.04 BT composition (whose SEM image is shown in Figure 2(c)) showed the highest porosity and irregular shaped unequal sized grains as compared with those of others. The SEM micrograph of 0.94 BNT-0.06 BT (Figure 2(e)) also shows slight porosity and inequality in grain size. Here it would not be inopportune to mention that BT has been fabricated under a different condition than that for $(1 - x)$BNT-xBT [21], and

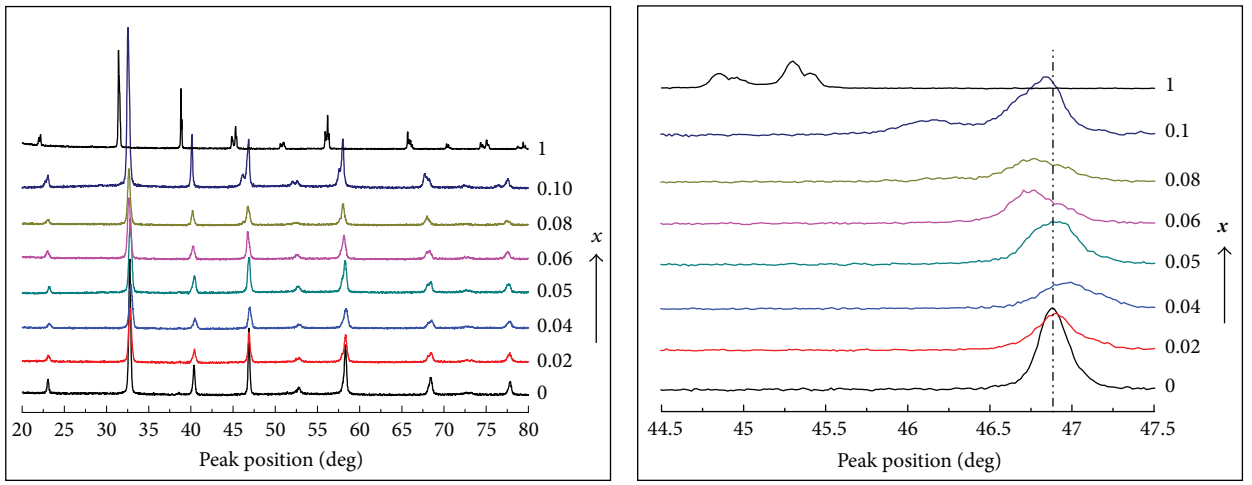

(a) (b)

Figure 1: (a) X-ray diffraction patterns and (b) expanded X-ray diffraction patterns of $(Bi_{0.5}Na_{0.5})_{1-x}Ba_xTiO_3$ ceramics (x = 0.0, 0.02, 0.04, 0.05, 0.06, 0.08, 0.10, and 1.0).

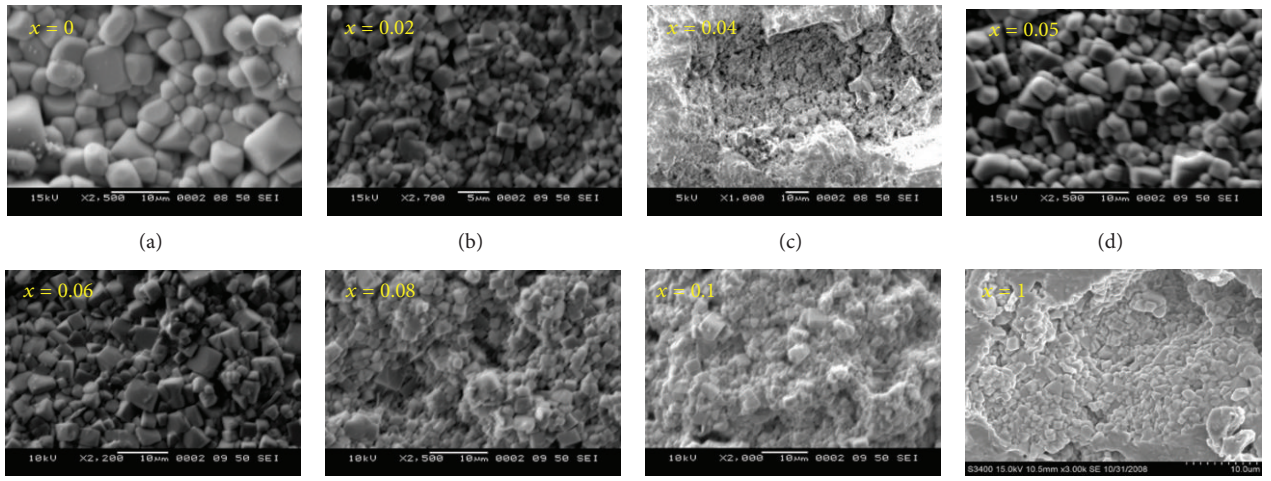

(a) (b) (c) (d)

(e) (f) (g) (h)

Figure 2: SEM micrographs of $(Na_{0.5}Bi_{0.5})_{1-x}Ba_xTiO_3$ (x = 0, 0.02, 0.04, 0.05, 0.06, 0.08, 0.10, and 1.0) compositions.

Table 1: The values of density, grain size, dielectric constant (ε_r), loss tangent ($\tan\delta$), and piezoelectric coefficient (d_{33}) at room temperature of $(Bi_{0.5}Na_{0.5})_{1-x}Ba_xTiO_3$ samples.

Samples	Density (g/cm^3)	Grain size (μm)	ε_r(RT/10 kHz)	$\tan\delta$ (RT/10 kHz)	d_{33} (pC/N)
BNT	4.85	3.51	673	0.26	17
0.98BNT-0.02BT	5.008	1.82	672	0.32	22
0.96BNT-0.04BT	5.078	2.97	545	0.11	50
0.95BNT-0.05BT	5.144	3.08	724	0.47	95
0.94BNT-0.06BT	5.234	3.01	871	0.08	124
0.92BNT-0.08BT	5.248	2.4	951	0.11	112
0.90BNT-0.10BT	5.382	2.76	1110	0.09	103
BT	6.02	1.6	1200	0.03	101 ± 5

the XRD data and SEM image for barium titanate have also been taken from the previous works of our group [21], and the value of longitudinal piezoelectric charge coefficient (d_{33}) for it has been taken from the literature [22] for comparison sake.

3.4. Piezoelectric Study. Minimum and maximum values of longitudinal piezoelectric charge coefficient (d_{33}) of the ceramic samples poled under an electric field of about 2.5 kV/mm in a silicone oil bath at 80°C/15 min were found to be ~17 pC/N and 124 pC/N for BNT and 0.94 BNT-0.06 BT compositions, respectively, as given in Table 1. A high value of d_{33} for 0.94 BNT-0.06 BT may be supposed to be due to the presence of morphotropic phase boundary (MPB) composition (where both monoclinic and tetragonal phases are supposed to coexist), as detailed before.

3.5. Complex Impedance Spectroscopic Analysis. Complex impedance spectroscopy (CIS) is a powerful tool for characterizing many of the electrical properties of materials and their interfaces with electronically conducting electrodes. It may be used to investigate the dynamics of bound or mobile charges in the bulk or interfacial regions of any kind of solid or liquid material: ionic, semiconducting, mixed electronic-ionic, and even insulators (dielectrics). An equivalent circuit based on impedance and electric modulus spectra provides the physical processes occurring inside the sample. Most of the real ceramics contain grains and grain-boundary regions, which individually have very different physical properties. These regions are well observed in the impedance and modulus spectra. The electrical properties of the present material system have been investigated using CIS technique. Electrical *ac* data may be presented in any of the four interrelated formalism: relative permittivity (ε^*) = $\varepsilon' - j\varepsilon''$; impedance ($Z^*$) = $Z' - jZ'' = 1/j\omega C_0\varepsilon^*$; electric modulus ($M^*$) = $M' + jM'' = 1/\varepsilon^*$; admittance ($Y^*$) = $Y' + jY'' = j\omega C_0\varepsilon^*$; and tan $\delta = \varepsilon''/\varepsilon' = M''/M' = Z'/Z'' = Y''/Y'$, where ω (= $2\pi f$) is the angular frequency; $C_0 = \varepsilon_0 A/t$ is the geometrical capacitance, $j = \sqrt{-1}$; ε_0 is the permittivity of free space (= 8.854×10^{-12} Fm^{-1}); $t$and A are the thickness and area of the pellet, respectively, and relative permittivity (ε') = C_p/C_0. Here, C_p is the parallel capacitance, and δ, the loss angle, is the complementary (=90 − θ) to the phase angle (θ), both of which are directly observed by the LCR Hi-Tester. The modulus ($|Z|$) of the complex impedance (Z^*) is directly observed by the LCR Hi-Tester so that $Z\cos\theta$ (= Z') and $Z\sin\theta$ (= Z''), respectively, give the real and imaginary parts of the impedance (Z^*). The frequency dependence of Z' for $(1-x)$BNT-xBT (x = 0, 0.02, 0.04, 0.05, 0.06, 0.08, and 1) ceramics, at several temperatures between ambient temperature and 450°C is observed (but not shown by plots, for brevity sake). At lower temperatures, Z' decreases monotonically with increasing frequency up to a certain frequency and then becomes frequency-independent. Only at the highest chosen temperature, that is, at 450°C, $Z'(f)$ plots tend to provide peaks below the lowest measurement frequency range, that is, 100 Hz. The higher values of Z' at comparatively lower frequencies and lower temperatures mean that the polarization in the test material is larger under the aforesaid conditions. The temperature where this change occurs varies with frequency in different materials. This also means that the resistive grain-boundaries become conductive at these temperatures. This also shows that the grain-boundaries are not relaxing even at very high frequencies and higher temperatures. $Z''(f)$ plots (although not shown in the present paper, for brevity sake) showed almost identical monotonically decreasing type of variation up to a certain frequency limit beyond which they merge together to show frequency-independent nature of variation extending up to the highest frequency limit at all the chosen temperatures, except at the highest one, that is, at 450°C, in which case all the $Z''(f)$ plots give peaks in the limiting frequency range of ~122 Hz–364 Hz for 0.94 BNT-0.06 BT and BNT, respectively, as shown in Figure 3. However, barium titanate (dopant) concentration-dependent shifting of $Z''(f)$ either towards higher or lower frequency side could not be clearly affirmed from the plots. Further, no peaks were seen for 0.96 BNT-0.04 BT and 0.90 BNT-0.10 BT compositions. The merger of Z'' (as well as of Z') at higher frequencies for all the temperatures indicates possible release of space charge polarization/accumulation at the boundaries of homogeneous phases in the applied external field. At lower temperatures, Z'' decreases monotonically, thereby suggesting that the relaxation in the material system at lower temperatures is absent. This means that relaxation species are immobile defects, and the orientation effects may be associated. Also, the magnitude of Z' and Z'' decreases with increasing frequencies. This would imply that relaxation in the material system is temperature-dependent, and there is apparently not a single relaxation time. The electrical behavior of the system has been studied over a wide range of temperature 35–450°C and frequency 100 Hz–1 MHz. In order to study the contribution of various microscopic elements such as intragrain, intergrain, electrode effect, and relaxation process, we have used the Cole-Cole plots analysis. Figures 4(a) through 4(g) shows the Cole-Cole plots of the compounds at different temperatures only 375–450°C and the plot corresponding to 450°C for different $(1 - x)$BNT-xBT compositions is shown in Figure 4(h). From the data it is apparent that, at low temperatures, when the resistivities of the samples are too high, a small portion of the impedance dispersion profile can be detected in the measured frequency range and thus making data analysis impossible. Since the impedance measurements performed for all the samples below 375°C did not present a complete semicircle, they could not be considered for equivalent circuit modeling in this study. It can be seen that the semicircles exhibit their depressed centers below the abscissa representing the distribution of relaxation times. This nonideal behavior could be attributed to the several factors such as grain orientation, grain-boundary, stress-strain phenomena, and atomic defect distribution. A series array of two parallel RC combinations $[(R_g, C_g), (R_{gb}, C_{gb})]$ in series with a resistor (R_s) (though the data of R_s for any of the samples are not shown in the table, for brevity sake) was found to best fit the experimental data for all the samples, thereby indicating the contribution from grain of the sample in the high frequency region and from the grain-boundaries in the low frequency region. No other relaxation

Table 2: Grain (bulk)/(grain-boundary) resistances (R_g/R_{gb}), capacitances (C_g/C_{gb}), and the corresponding relaxation times (τ_g/τ_{gb}) at 450°C for $(1-x)$BNT-xBT ceramic.

Composition	R_g	R_{gb}	C_g	C_{gb}	τ_g	τ_{gb}
BNT	0.28 MΩ	0.47 MΩ	1.12 nF	1.14 nF	0.34 ms	0.54 ms
0.98BNT-0.02BT	0.68 MΩ	0.97 MΩ	0.69 nF	0.82 nF	0.47 ms	0.80 ms
0.96BNT-0.04BT	8.91 MΩ	—	—	—	—	—
0.95BNT-0.05BT	0.16 MΩ	0.29 MΩ	0.03 nF	1.73 nF	4.00 μs	0.50 ms
0.94BNT-0.06BT	0.22 MΩ	0.49 MΩ	0.62 nF	2.46 nF	0.14 ms	1.17 ms
0.92BNT-0.08BT	0.18 MΩ	0.32 MΩ	0.003 nF	2.64 nF	0.47 μs	0.86 ms
0.90BNT-0.10BT	0.35 MΩ	0.63 MΩ	2.11 nF	2.16 nF	0.74 ms	1.36 ms

mechanism, such as the electrode effects, is identified in the studied frequency range. Table 2 shows the barium titanate (dopant) concentration dependent variation of grain (bulk or intrinsic) and grain-boundary related relaxation times τ_g $(= R_g * C_g)$ and $\tau_{gb}(= R_{gb} * C_{gb})$ for $(1-x)$BNT-xBT compositions. R_g and R_{gb} at the specified temperature are evaluated from the intercepts of the corresponding semicircles on the Z'-axis that is, from the semicircle diameter, while C_g and C_{gb} are evaluated from the values of frequency at the peaks $(= f_{max})$ in the $Z''(f)$ plots by using the relation $\omega_m\tau_m = 1$, that is, $\omega_{max} = 1/RC$ because f_{max} corresponds to the relaxation frequency. Evaluated parameters using the above relations show that.for BNT and 0.98 BNT-0.02 BT both the time periods tend to increase while they decrease in the case of 0.95 BNT-0.05 BT. τ_g continuously increases to reach a maximum value of 0.74 ms for 0.90 BNT-0.10 BT composition, and τ_{gb} also reaches a maximum value of 1.36 ms for 0.90 BNT-0.10 BT composition, but for the compositions in between 0.95 BNT-0.05 BT, and 0.90 BNT-0.10 BT it shows an increasing, decreasing, and then again increasing trends with increasing concentration of dopant (barium titanate) in different compositions.

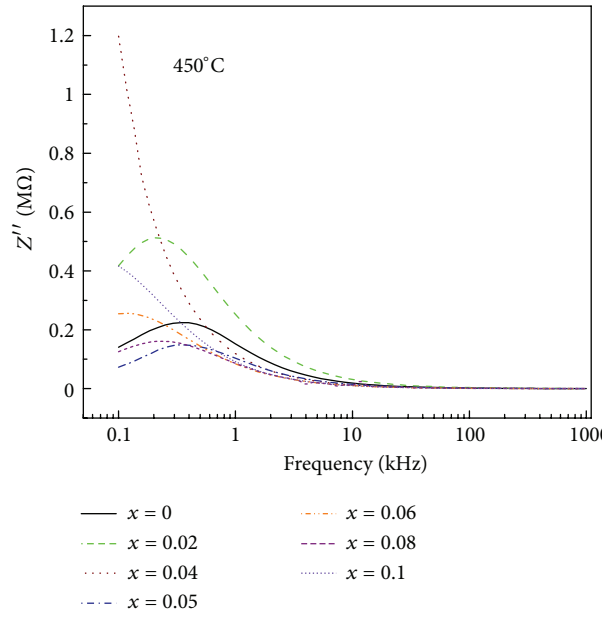

Figure 3: Frequency dependence of Z'' of $(1-x)$BNT-xBT ($x = 0$, 0.02, 0.04, 0.05, 0.06, 0.08, and 1) ceramics, at 450°C.

3.6. Complex Modulus Analysis. Complex modulus formalism is a very important and convenient alternative tool for impedance spectroscopy with additional advantages as compared to those in complex impedance spectroscopy (CIS) in determining, analyzing, and interpreting the dynamical aspects of electrical transport phenomena (i.e., parameters such as carrier/ion hopping rate, and conductivity relaxation time). It provides an insight into the electrical processes characterized by the smallest capacitance of the material. In order to analyze and interpret experimental data, it is essential to have a model equivalent circuit that provides a realistic representation of the electrical properties. The modulus representation suppresses the unwanted effects of extrinsic relaxation often used in the analysis of dynamic conductivities of ionically conducting glasses and is also frequently used in the analysis of dielectric data of ionic conductors [23]. The advantage of adopting complex electrical modulus spectra is that it can discriminate against electrode polarization and grain-boundary conduction process. Using electric modulus analysis, it is easier to relate this phenomenon to other properties, especially the dynamical mechanical modulus, and can be written as a single function of conductivity. Moynihan et al. [24] and Moynihan [25] have given detailed analyses of the electric modulus formalism and application of the Kohlrausch decay function. The Kohlrausch-Williams-Watts (KWW) function, which in our case will be the Kohlrausch electrical relaxation function is given by $\varphi(t) = \exp[-(t/\tau)^{\beta}]$, with $0 < \beta < 1$. For a realistic assessment of the modulus formalism, it is important to realize that it is based on the description of electric response of the sample in terms of the macroscopic field decay function $\varphi(t)$. Empirically, the KWW function is a convenient choice for $\varphi(t)$, and the nonexponential parameter β is suitably varied to fit the data. The peak position of frequency in loss modulus spectra gives the most probable relaxation time from the condition $\omega_m\tau_m = 1$, as detailed under the section of CIS. The most probable relaxation time also obeys the Arrhenius relation $\omega_m = \omega_o\exp(-E_a/k_BT)$. From the spectra it can be observed that below the Curie temperature bulk properties of ceramic samples come from the grain capacitance of the materials. Semicircles were drawn by fitting the data points manually. Two distinguished semicircles could be drawn

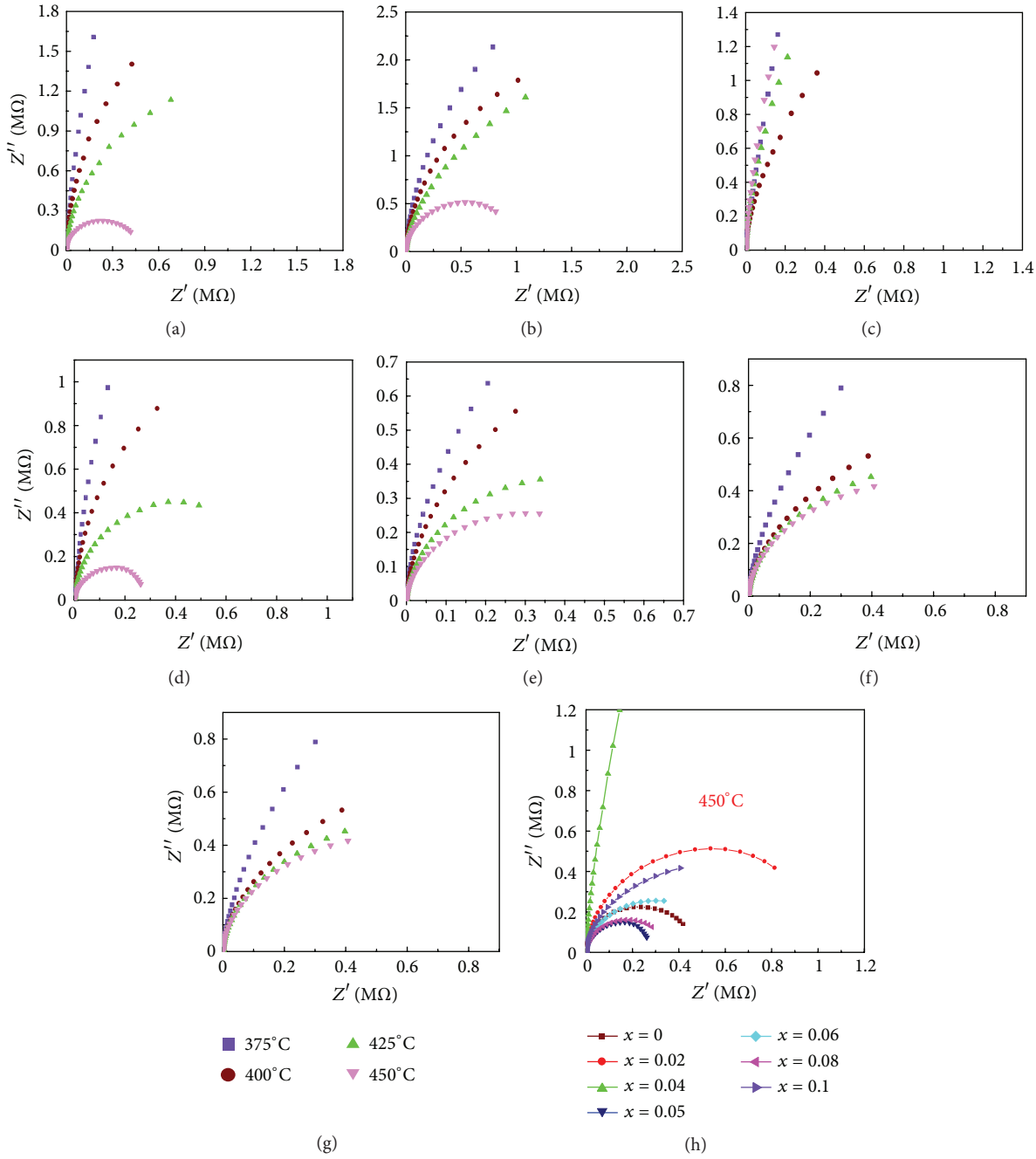

FIGURE 4: (a)–(g) Complex impedance plots for $(1-x)$BNT-xBT (x = 0, 0.02, 0.04, 0.05, 0.06, 0.08, and 1) ceramics at different temperatures and (h) corresponding plots at 450°C.

above the Curie temperature, specifically at 450°C, for all the test material system (as depicted in Figures 5(a) through 5(f), except for the case of 0.98 BNT-0.02 BT as shown in Figure 5(b) in which a lone semicircle corresponding to the grain-boundary was observed). In this type of formulism, the left semicircle represents the grain-boundary while the right one corresponds to the bulk or the grains inside the test material. These semicircles indicate that both grain and grain-boundary capacitance started active role in the conduction mechanism above the Curie temperature, that is, in the paraelectric phase of the material system. However, no modulus spectrum could be drawn for 0.96 BNT-0.04 BT, possibly due to the inhomogeneous and porous nature of the sample as evidenced by the SEM image too. Under the said condition, we could not perform the fitting analysis for the data points in the light of KWW function because no prominent peaks for frequency-dependent imaginary part of electric modulus ($M''(f)$) spectra corresponding to different temperatures, except at ~400–450°C, were seen for our test material system in the specified measurement

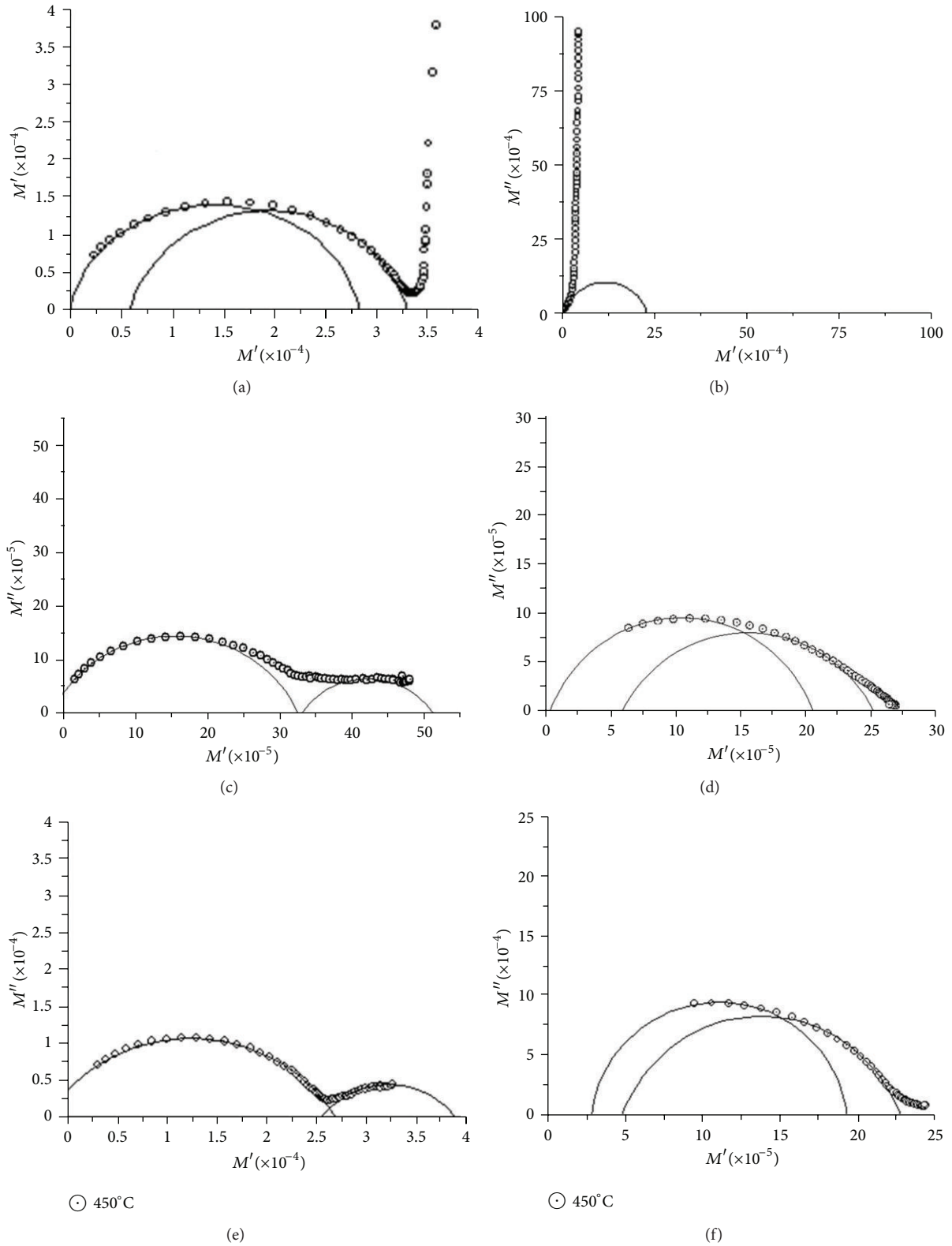

Figure 5: (a)–(f) The Nyquist plots in the complex electric modulus plane for $(1 - x)$BNT-xBT ($x = 0$, 0.02, 0.04, 0.05, 0.06, 0.08, and 1) ceramic samples corresponding to the data for M' and M'' at 450°C.

ranges of temperature and frequency. From the Nyquist plots in the complex electric modulus plane corresponding to 450°C it transpired that for undoped BNT grain-boundaries and grains exhibit almost equal contributions and with an increase in the content of the dopant barium titanate, the grain contribution appears to diminish with simultaneous enhancement in grain-boundary contribution, and this effect continues up to the case of 0.92 BNT-0.08 BT, that is, near the MPB composition beyond which again an enhancement in contribution due to grains is seen (as depicted in Figure 5(f)). Further, the two semicircles appear most separated from each other for the case of 0.95 BNT-0.05 BT (as shown in Figure 5(c)).

3.7. Conductivity Analysis. The real part of ac conductivity is calculated by using the expression

$$\sigma'_{\text{ac}} = \varepsilon' \varepsilon_{\circ} \omega \tan \delta, \tag{2}$$

where ω (= $2\pi f$) is the cyclic frequency f (being the frequency of measurement), ε_0 is the free space permittivity (= 8.85×10^{-12} Fm^{-1}), ε' is the dielectric constant (= C_p/C_0, as detailed earlier under CIS section) and tanδ is the dielectric loss tangent for the test material sample. Figures 6(a)–6(g) show the log-log plot of ac electrical conductivity (σ'_{ac}) versus frequency at different temperatures. It is observed from these plots (Figure 6) that, in the low temperature regime, ac conductivity increased with increase in frequency, thereby indicating dispersion of conductivity with frequency. With increase in temperature, dispersion in conductivity narrowed down, and all the curves for different frequencies appeared to merge at high temperatures, although they did not merge completely. The activation energy for conduction was obtained using the Arrhenius relationship:

$$\sigma_{\text{ac}} = \sigma_o \exp\left(\frac{-E_a}{k_B T}\right). \tag{3}$$

A linear least-squares-fit of the conductivity data to (3) gives the value of the apparent activation energy, E_a. The ac activation energies were calculated in two different temperature regions at different frequencies, and the values are given in Table 3. The activation energy values for ac conductivity are found to increase with the increase in temperature. It is also observed that ac conductivity-based activation energy calculated at higher frequencies is lower than that at lower ones in the same temperature range for all the compositions, albeit not shown in the present work for brevity sake. This is due to the fact that at low frequencies the overall conductivity is due to the mobility/transportation of charge carriers over long distance rather than from relaxation/orientational mechanism, in which case charge mobility/transportation is restricted to only the nearest neighbouring lattice sites. The conductivity of the materials has been found to increase with increase in temperature, and merging of the conductivity curves in the higher temperature region results with the release of space charge, thereby endorsing the results derived from the complex impedance spectroscopic analyses. In the low temperature region (35–300°C), the activation energies for $(1-x)$BNT-xBT system (where x = 0, 0.02, 0.04, 0.05, 0.06, 0.08 and 1) are in the range of 0.015–0.16 eV. In this region, conductivity is almost independent of temperature, and this low value of activation energy corresponds to the intrinsic conduction in the test material system. The activation energies ~0.11–0.47 eV in the second temperature region (325–450°C) were slightly increased with an increase in temperature, thereby suggesting that the conductivity may be the result of defects and associated charge carriers of metal ions such as Na^+, Bi^{3+}, and Ba^{2+}. At high sintering temperatures, bismuth ions are the first to get evaporated, and thereby oxygen vacancies are created for charge neutralization. Defects such as bismuth $V_{\text{Bi}}^{\bullet\bullet\bullet}$ and oxygen vacancies $V_O^{\bullet\bullet}$ are considered to be the most mobile charges and play an important role in polarization fatigue and conduction [26]. The estimated activation energies of the material system may correspond to the motion of oxygen vacancies in the octahedron of the perovskite structures. The dc conductivity study can help to illustrate not only the effects of grain orientation, but also the nature of charge carriers. Approximate values of dc conductivity of the test materials were evaluated from the extrapolation of the available plateaus of the $\sigma_{\text{ac}}(\omega)$ plots up to $\omega = 0$ corresponding to 350°C, 400°C, and 450°C. For the study of temperature-dependent variation of dc conductivity, the following formula was used

$$\sigma_{\text{dc}} = \left(\frac{\sigma_o}{T}\right) \exp\left(\frac{-E_a}{k_B T}\right). \tag{4}$$

The slope of the $\ln(\sigma^*_{\text{dc}}T)$ versus 10^3/T plots yielded the values of activation energy for dc conductivity (E_a) as given in Table 3. In the high temperature regime, the slopes rapidly increased with an increase in temperature. The calculated activation energies of $(1-x)$BNT-xBT (where x = 0.0, 0.02, 0.04, 0.05, 0.06, 0.08, and 0.1) ceramics in this region are 1.416, 1.011, 0.539, 1.447, 0.771, 1.304, and 0.783 eV, respectively. As reported earlier [27, 28], motion of oxygen vacancies in the octahedron of any perovskite structure gives rise to an activation energy ~1.10 eV. On the basis of the above analyses, it can be concluded that the dc conductivity in the higher temperature regime is due to motion of oxygen vacancies across the grain-boundary. Thus, we see that at higher temperatures dc conductivity is more dominant in the studied material system. This is reminiscent of the semiconducting behavior of the material system, as mentioned earlier.

In a bid to extend our frequency-dependent ac conductivity study, the double power law, the generalized version of Jonscher's power law

$$\sigma_{\text{ac}} = \sigma_o + A\omega^{S_1} + B\omega^{S_2} \tag{5}$$

is to be used.

Here σ_o is the frequency-independent (electronic or dc) part of ac conductivity. Further, the exponent s_1 ($0 \le s_1 \le 1$) characterizes the low frequency region, corresponding to translational ion hopping, and the exponent s_2 ($0 < s_2 < 2$) characterizes the high frequency region, indicating the existence of well-localized relaxation/reorientational process [29], the activation energy of which is ascribed to reorientation ionic hopping. Almond has proposed a different

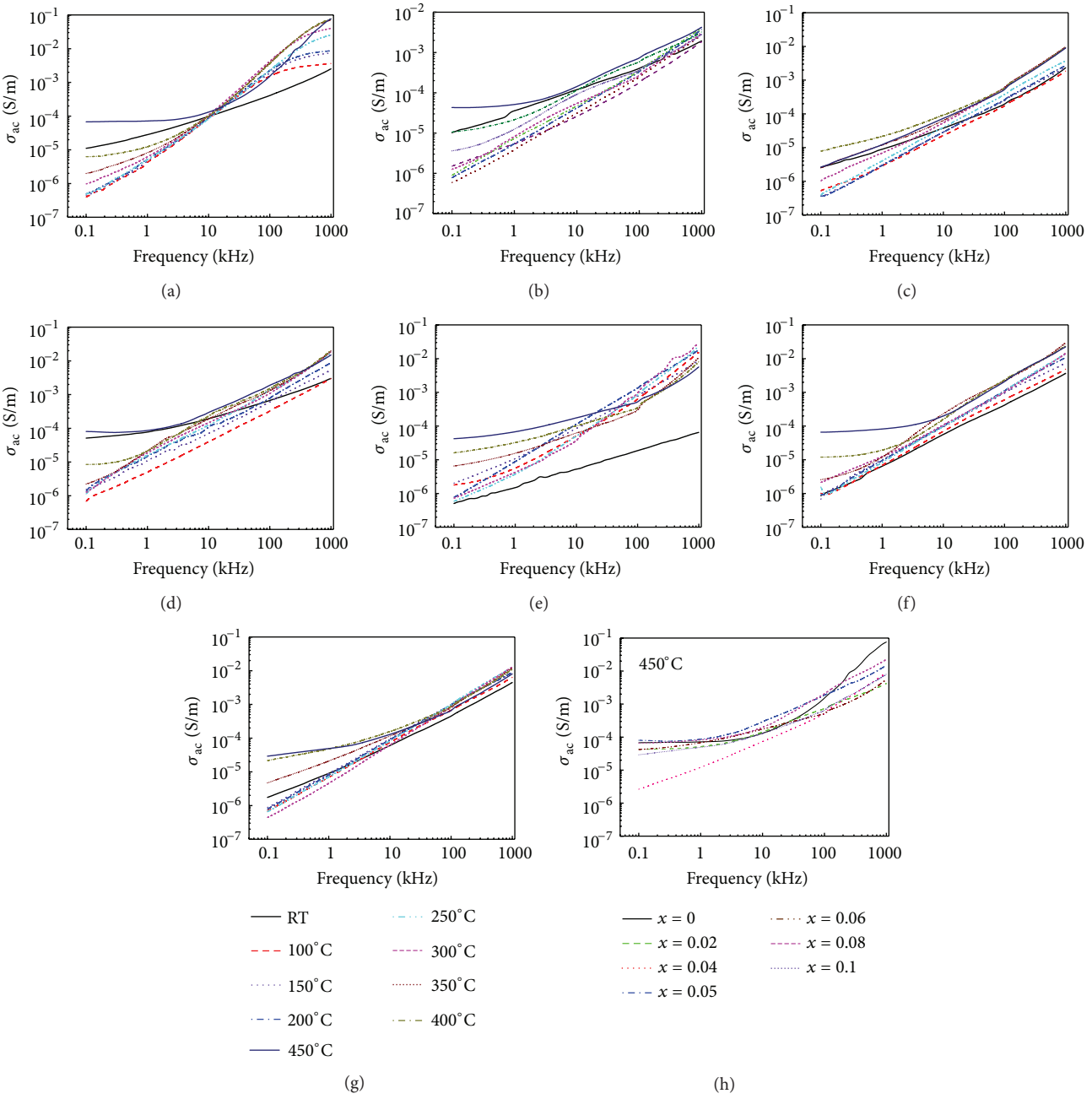

Figure 6: (a)–(g) Frequency dependence of real part of complex ac conductivity for $((BNT)BT)_x$ (x = 0, 0 02, 0.04, 0.05, 0.06, 0.08, and 1) ceramics at several temperatures and (h) corresponding plots at 450°C.

Table 3: ac/dc conductivity-based activation energy for different compositions in the low and high temperature ranges.

Composition	ac activation energy (eV) in low temp. region (35°C–300°C)	ac activation energy (eV) in high temp. region (325°C–450°C)	dc activation energy (eV) in high temp. region (350°C–450°C)
BNT	0.148	0.144	1.416
0.98BNT-0.02BT	0.164	0.114	1.011
0.96BNT-0.04BT	0.015	0.158	0.539
0.95BNT-0.05BT	0.112	0.138	1.447
0.94BNT-0.06BT	0.140	0.316	0.771
0.92BNT-0.08BT	0.047	0.169	1.304
0.90BNT-0.10BT	0.072	0.477	0.783

approach in which microstructural network in the system is responsible for this power law behavior [30, 31]. Hopping model is extensively studied over a wide range of materials like ceramics, polymers, composites, and so forth and can successfully explain the double power law behavior, the particular case $n > 1$ [32], and so forth in these materials. Further, it may be inferred that the slope s_1 is associated with grain-boundary conductivity, whereas s_2 depends on grain conductivity [29]. In the jump relaxation model (JRM) introduced by Funke [29] and extended by Elliot [33] to account for ionic conduction in solids, there is a high probability for a jumping ion to jump back (unsuccessful hop). However, if the neighborhood becomes relaxed with respect to the ion's position, the ion stays in the new site. The conductivity in the low frequency region is associated with successful hops. Beyond the low frequency region, many hops are unsuccessful, and as the frequency increases, more hops are unsuccessful. The change in the ratio of successful to unsuccessful hops results in dispersive conductivity. In the perovskite type oxide materials, presence of charge traps in the band gap of the insulator is expected. The JRM suggests that different activation energies are associated with unsuccessful and successful hopping processes. The frequency and temperature-dependence of ac conductivity in the $(1 - x)$BNT-xBT system of materials resembles that of hopping type conduction. Applying JRM to the frequency response of the conductivity for the test materials, experimental inverse temperature-dependent conductivity data, as shown in Figure 7 were found to fit the double power law as given in (5). The temperature-dependent variations of the exponents, s_1 and s_2, are shown in Figures 8(a) through 8(g). From the plots (Figure 8(b)), it is manifested that s_1 assumes a maximum value ~1.243 at 100°C for 0.98 BNT-0.02 BT and s_2 assumes a maximum value ~1.746 at 450°C for the same composition. Further, peaks were seen to appear only near T_m (i.e., the antiferroelectric/paraelectric phase transition temperature) for almost all the material compositions. However, in some of the compositions, the peaks were sharper while in some others they were flat, that is, plateau-like. To be more specific, BNT exhibits plateau both for $s_1(T)$ and $s_2(T)$ in the temperature range 100–300°C; in the 0.98 BNT-0.02 BT composition, $s_2(T)$ shows a monotonically increasing trend while $s_1(T)$ shows a plateau between the same temperature limits; 0.96 BNT-0.04 BT shows a trough for $s_1(T)$ at ~400°C; 0.95 BNT-0.05 BT exhibits shoulders at ~100°C and flat peaks at ~300°C both for $s_1(T)$ and $s_2(T)$. Furthermore, $s_1(T)$ and $s_2(T)$ in 0.94 BNT-0.06 BT (assumed MPB composition) show almost the same trend of variation as in 0.95 BNT-0.05 BT with the only difference that in this case the $s_2(T)$ peak shifts towards higher temperature side while $s_1(T)$ peak shifts towards opposite side and beyond the MPB composition that is, for 0.92 BNT-0.08 BT, the peaks show opposite shifting as compared with that in the MPB composition. Lastly, for 0.90 BNT-0.10 BT composition the trends for the variation of $s_1(T)$ and $s_2(T)$ are the same as in the MPB composition. As shown in Figure 8(e), the minimum values of both $s_1(= 0.516)$ and $s_2(= 0.545)$ are exhibited by the 0.94 BNT-0.06 BT composition at 35°C, that is, at the temperature of ambience. Due to localization

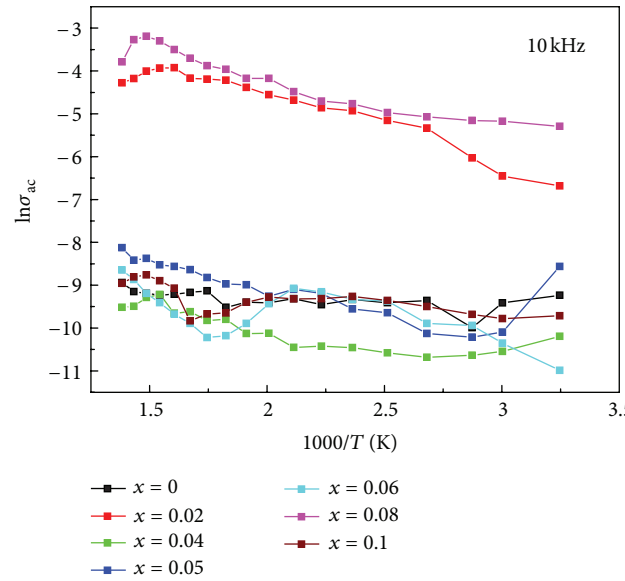

FIGURE 7: Inverse temperature-dependent variation of ln (real part of complex ac conductivity) for $(1 - x)$BNT-xBT ($x = 0$, 0.02, 0.04, 0.05, 0.06, 0.08, and 1) ceramics at 10 kHz.

of charge carriers, formation of polarons takes place, and the hopping conduction may occur between the nearest neighboring sites. As referred to earlier, the enhancement in conductivity with temperature may be considered on the basis that within the bulk the oxygen vacancies due to the loss of oxygen (usually created during sintering) allow the charge compensation process to occur which follows the Kröger-Vink equation [34] in the form $O_o \rightarrow (1/2)O_2 \uparrow + V_o^{\bullet\bullet} + 2e^{-1}$ thereby showing that free electrons are left behind in the process, making the materials n-type. It may further be opined that lower high frequency ac activation energy than that at low frequency may possibly be due to the fact that at low frequencies the overall conductivity is due to the mobility/transportation of charge carriers over long distance rather than relaxation/orientational mechanism, in which case charge mobility/transportation is restricted to only the nearest neighboring lattice sites. Higher values of conductivity based activation energy at lower frequencies than those at higher ones are obtained due to the fact that the energy required for relaxation/orientational process is lower than that required for mobility of charge carriers over a long distance. In the light of the resulting frequency- and temperature-dependent ac conductivity data for $(1 - x)$BNT-xBT ceramic samples, it may be inferred that JRM has shown its applicability in the entire frequency range for the test material system.

4. Conclusion

The present work describes the piezoelectric, impedance, and conductivity studies of $(Na_{0.5}Bi_{0.5})_{1-x}Ba_xTiO_3$; $(1 - x)$BNT-xBT ($0 \leq x \leq 1$) ceramics. X-ray diffraction data confirmed the formation of phase pure compounds in all the compositions and the apparent crystallite (particle)

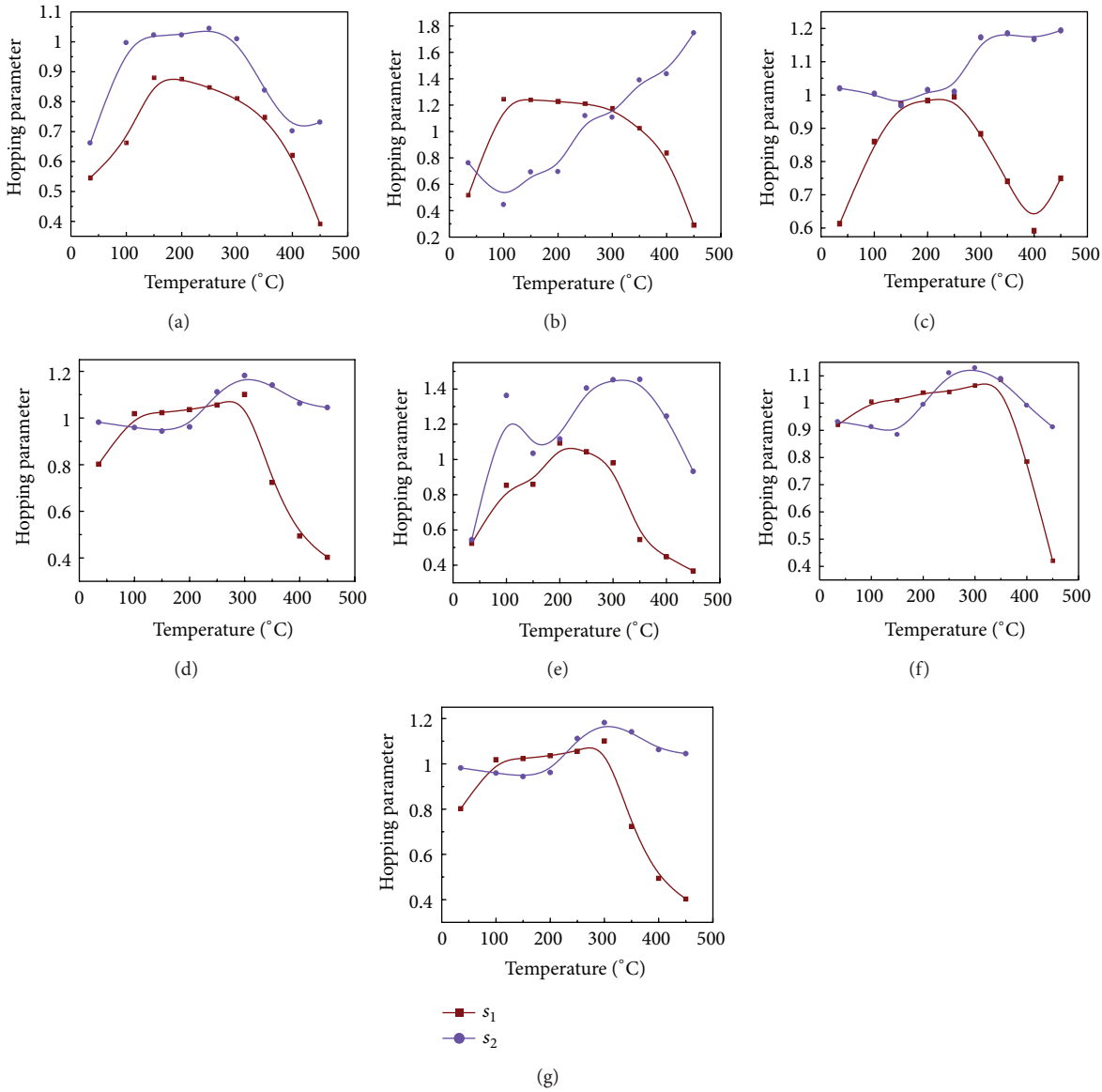

FIGURE 8: (a)–(g) Temperature-dependence of low and high frequency hopping parameters (s_1 and s_2) for $(1-x)$BNT-xBT ($x = 0$, 0.02, 0.04, 0.05, 0.06, 0.08, and 1) ceramics between ambient temperature and 450°C.

sizes are in the ~26–52 nm range. SEM micrographs showed grain sizes ranging 1.8–3.5 μm and the relative densities in the range of 91–97% of the theoretical ones in all the compositions. Values of longitudinal piezoelectric charge coefficients of the $(1-x)$BNT-xBT samples poled under a dc electric field of about 2.5 kV/mm at 80°C/15 min lie in the range of 17–124 pC/N. Complex impedance analysis in the frequency range 100 Hz–1 MHz over a wide temperature range 35°C–450°C indicates the presence of grain-boundary effect along with the bulk contribution and also confirms the presence of the non-Debye type of multiple relaxations in the materials. Conduction mechanism in the material system is explained on the basis of jump relaxation hopping model of charge carriers. The electrical conductivity measurements with temperature suggest the negative temperature coefficient of resistance behaviour for the material system. The ac/dc conduction-based activation energies for the test material system have also been estimated. The present study of $(1-x)$BNT-xBT ($0 \leq x \leq 1$) ceramics is assumed worthwhile in probing the conduction mechanism in detail which may be helpful in tailoring the electrical characteristics for desired applications.

Acknowledgments

The authors gratefully acknowledge the financial support by the Department of Science and Technology, New Delhi, under Grant no.SR/S2/CMP-017/2008. Thanks are also due to Professor Nawal Binhayeeniyi et al. for the help taken in the present work for comparison purposes from [22].

References

[1] G. A. Smolenskii, V. A. Isupov, A. I. Agranovskaya, and N. N. Krainik, "New ferroelectrics of complex composition," *Soviet Physics, Solid State*, vol. 2, pp. 2651–2654, 1961.

[2] A. Hussain, C. W. Ahn, H. J. Lee et al., "Anisotropic electrical properties of $Bi_{0.5}(Na_{0.75}K_{0.25})_{0.5}TiO_3$ ceramics fabricated by reactive templated grain growth (RTGG)," *Current Applied Physics*, vol. 10, pp. 305–310, 2010.

[3] D. Z. Zhang, X. J. Zheng, X. Feng et al., "Ferro-piezoelectric properties of $0.94(Na_{0.5}Bi_{0.5})TiO_3$-$0.06BaTiO_3$ thin film prepared by metal-organic decomposition," *Journal of Alloys and Compounds*, vol. 504, no. 1, pp. 129–133, 2010.

[4] C. Ma and X. Tan, "Phase diagram of unpoled lead-free (1-x)$(Bi_{1/2}Na_{1/2})TiO_3$-x$BaTiO_3$ ceramics," *Solid State Communications*, vol. 150, no. 33-34, pp. 1497–1500, 2010.

[5] Z. Yang, B. Liu, L. Wei, and Y. Hou, "Structure and electrical properties of $(1-x)Bi_{0.5}Na_{0.5}TiO_3$-$xBi_{0.5}K_{0.5}TiO_3$ ceramics near morphotropic phase boundary," *Materials Research Bulletin*, vol. 43, no. 1, pp. 81–89, 2008.

[6] W. C. Lee, C. Y. Huang, L. K. Tsao, and Y. C. Wu, "Crystal Structure, dielectric and ferroelectric properties of $(Bi_{0.5}Na_{0.5})TiO_3$-$(Ba,Sr)TiO_3$ lead-free piezoelectric ceramics," *Journal of Alloys and Compounds*, vol. 492, no. 1-2, pp. 307–312, 2010.

[7] D. Lin, K. W. Kwok, and H. L. W. Chan, "Ferroelectric and piezoelectric properties of $Bi_{0.5}Na_{0.5}TiO_3$-$SrTiO_3$-$Bi_{0.5}Li_{0.5}TiO_3$ lead-free ceramics," *Journal of Alloys and Compounds*, vol. 481, no. 1-2, pp. 310–315, 2009.

[8] Z. Yang, Y. Hou, H. Pan, and Y. Chang, "Structure, microstructure and electrical properties of $(1-x-y)Bi_{0.5}Na_{0.5}TiO_3$-$xBi_{0.5}K_{0.5}TiO_3$-$yBi_{0.5}Li_{0.5}TiO_3$ lead-free piezoelectric ceramics," *Journal of Alloys and Compounds*, vol. 480, no. 2, pp. 246–253, 2009.

[9] M. Zou, H. Fan, L. Chen, and W. Yang, "Microstructure and electrical properties of $(1-x)[0.82Bi_{0.5}Na_{0.5}TiO_3$-$0.18Bi_{0.5}K_{0.5}TiO_3]$-$x$$BiFeO_3$ lead-free piezoelectric ceramics," *Journal of Alloys and Compounds*, vol. 495, no. 1, pp. 280–283, 2010.

[10] S.-T. Zhang, B. Yang, and W. Cao, "The temperature-dependent electrical properties of $Bi_{0.5}Na_{0.5}TiO_3$-$BaTiO_3$-$Bi_{0.5}K_{0.5}TiO_3$ near the morphotropic phase boundary," *Acta Materialia*, vol. 60, no. 2, pp. 469–475, 2012.

[11] H. Ni, L. Luo, W. Li, Y. Zhu, and H. Luo, "Preparation and electrical properties of $Bi_{0.5}Na_{0.5}TiO_3$-$BaTiO_3$-$KNbO_3$ lead-free piezoelectric ceramics," *Journal of Alloys and Compounds*, vol. 509, no. 9, pp. 3958–3962, 2011.

[12] M. L. Liu, D. A. Yang, and Y. F. Qu, "Study on Bi_2O_3 doping methods and dielectric property of $(1-x)BaTiO_3$-$x(Bi_{0.5}Na_{0.5})TiO_3$ ceramics," *Journal of Alloys and Compounds*, vol. 496, no. 1-2, pp. 449–453, 2010.

[13] T. Takenaka, T. Okuda, and K. Takegahara, "Lead-free piezoelectric ceramics based on $(Bi_{1/2}Na_{1/2})TiO_3$-$NaNbO_3$," *Ferroelectrics*, vol. 196, no. 1–4, pp. 175–178, 1997.

[14] K. H. Ryu, T. K. Song, M. Kim et al., "Effect of $BiFeO_3$ doping on ferroelectric and piezoelectric properties of $(Bi_{0.5}Na_{0.5})TiO_3$ and $BATiO_3$ ceramics," *Integrated Ferroelectrics*, vol. 84, no. 1, pp. 31–38, 2006.

[15] H. Nagata and T. Takenaka, "Lead-free piezoelectric ceramics of $(Bi_{1/2}Na_{1/2})TiO_3$-1/2$(Bi_2O_3{\cdot}Sc_2O_3)$ system," *Japanese Journal of Applied Physics, Part 1*, vol. 36, no. 9, pp. 6055–6057, 1997.

[16] A. Herabut and A. Safari, "Processing and electromechanical properties of $(Bi_{0.5}Na_{0.5})_{(1-1.5x)}La_xTiO_3$ ceramics," *Journal of the American Ceramic Society*, vol. 80, no. 11, pp. 2954–2958, 1997.

[17] X. Wang, H. L. W. Chan, and C. L. Choy, "$(Bi_{1/2}Na_{1/2})TiO_3$-$Ba(Cu_{1/2}W_{1/2})O_3$ lead-free piezoelectric ceramics," *Journal of the American Ceramic Society*, vol. 86, no. 10, pp. 1809–1811, 2003.

[18] M. Rawat, K. L. Yadav, A. Kumar, P. K. Patel, N. Adhlakha, and J. Rani, "Structural, dielectric and conductivity properties of Ba^{2+} doped $(Bi_{0.5}Na_{0.5})TiO_3$ ceramic," *Advanced Materials Letters*, vol. 3, no. 4, pp. 286–292, 2012.

[19] C. Suryanarayan and M. G. Nortan, *X-Ray Diffraction a Practical Approach*, Plenum Press, New York, NY, USA, 1998.

[20] O. Muller and R. Roy, *The Major Ternary Structural Families*, Springer, New York, NY, USA, 1974.

[21] K. AmarNath and K. Prasad, "Structural and electrical properties of perovskite $Ba(Sm_{1/2}Nb_{1/2})O_3$-$BaTiO_3$ ceramic," *Advances in Materials Research*, vol. 1, no. 2, pp. 115–128, 2012.

[22] N. Binhayeeniyi, P. Sukvisut, C. Thanachayanont, and S. Muensit, "Physical and electromechanical properties of barium zirconium titanate synthesized at low-sintering temperature," *Materials Letters*, vol. 64, no. 3, pp. 305–308, 2010.

[23] N. G. McCrum, B. E. Read, and G. Williams, *Anelastic and Dielectric Effects in Polymeric Solids*, John Wiley & Sons, New York, NY, USA, 1967.

[24] C. T. Moynihan, "Analysis of electrical relaxation in glasses and melts with large concentrations of mobile ions," *Journal of Non-Crystalline Solids*, vol. 172–174, no. 2, pp. 1395–1407, 1994.

[25] C. T. Moynihan, L. P. Boesch, and N. L. Laberge, "Decay function for the electric field relaxation in vitreous ionic conductors," *Physics and Chemistry of Glasses*, vol. 14, no. 6, pp. 122–125, 1973.

[26] W. L. Warren, K. Vanheusden, D. Dimos, G. E. Pike, and B. A. Tuttle, "Oxygen vacancy motion in perovskite oxides," *Journal of the American Ceramic Society*, vol. 79, no. 2, pp. 536–538, 1996.

[27] M. J. Forbess, S. Seraji, Y. Wu, C. P. Nguyen, and G. Z. Cao, "Dielectric properties of layered perovskite $Sr_{1-x}A_xBi_2Nb_2O_9$ ferroelectrics (A=La, Ca and $x = 0, 0.1$)," *Applied Physics Letters*, vol. 76, no. 20, pp. 2934–2936, 2000.

[28] A. K. Roy, A. Singh, K. Kumari, K. AmarNath, A. Prasad, and K. Prasad, "Electrical properties and ac conductivity of $(Bi_{0.5}Na_{0.5})_{0.5}Ba_{0.06}TiO_3$ ceramic," *ISRN Ceramics*, vol. 2012, Article ID 854831, 10 pages, 2012.

[29] K. Funke, "Jump relaxation in solid electrolytes," *Progress in Solid State Chemistry*, vol. 22, no. 2, pp. 111–195, 1993.

[30] D. P. Almond and C. R. Bowen, "Anomalous power law dispersions in ac conductivity and permittivity shown to be characteristic of microstructural electrical networks," *Physical Review Letters*, vol. 92, no. 15, Article ID 157601, 5 pages, 2004.

[31] C. R. Bowen and D. P. Almond, "Modelling the "universal" dielectric response in heterogeneous materials using microstructural electrical networks," *Materials Science and Technology*, vol. 22, pp. 719–724, 2006.

[32] G. Bator, "Ac and dc conductivity around the ferroelectric phase transition in $(CH_3NH_3)_3Bi_2Br_9$ (MABB) crystal," *Ferroelectrics*, vol. 200, no. 1–4, pp. 287–295, 1997.

[33] S. R. Elliot, "AC conduction in amorphous chalcogenide andpnictide semiconductors," *Advances in Physics*, vol. 36, pp. 135–217, 1987.

[34] F. A. Kröeger and H. J. Vink, "Relations between the concentrations of imperfections in crystalline solids," *Solid State Physics*, vol. 3, pp. 307–435, 1956.